

Parametric dependence of beam-ion-driven modes in NSTX and NSTX-U

E. D. Fredrickson, M. Podestá, R. Bell, A. Diallo, S. P. Gerhardt, B. LeBlanc, F. Levinton^a, H. Yuh^a

Princeton Plasma Physics Laboratory, Princeton New Jersey 08543

^aNova Photonics, Princeton, NJ 08543

eric@pppl.gov

Abstract. The International Tokamak Experimental Reactor (ITER) will have a large population of non-thermal, energetic ions consisting of fusion generated alphas and beam ions injected for current profile control. Potential redistribution and/or loss of those non-thermal ions is thus of concern as it will modify heating profiles, current profiles, and could lead to unacceptable heating of plasma facing components. Redistribution and losses of fast ions have been documented as resulting from multiple Alfvénic modes, Toroidal Alfvén Eigenmodes and energetic particle modes (fishbones) on many smaller plasma devices. This paper presents an empirical approach towards characterizing the stability boundaries for some of the common energetic-ion-driven instabilities seen on the National Spherical Torus Experiment (NSTX/NSTX-U), with a particular focus on Energetic Particle Modes (EPMs). New data from NSTX-U will be added to extend the parameter range in the database.

1. Introduction

This paper presents an empirical approach towards characterizing the stability boundaries for some of the common energetic-ion-driven instabilities seen on the National Spherical Torus Experiment (NSTX/NSTX-U) [1]. The previous work is expanded here by including q and rotation profile information. NSTX-U data will also be added, and some discussion of new results from NSTX-U will be included. Understanding the conditions for which beam-driven instabilities arise, and the extent of the resulting perturbation to the fast-ion population, is important for predicting and eventually demonstrating non-inductive current ramp-up and sustainment in NSTX-U, as well as the performance of future fusion plasma experiments such as ITER. Data on energetic particle driven modes from NSTX provides the valuable service of challenging theoretical models for mode stability.

In previous work [2], a database was constructed based on shots from the 2010 NSTX experimental campaign for which TRANSP runs were performed. Each shot was divided into 50 ms intervals and the dominant beam-driven activity in each interval was characterized. Plasma parameters, including the central Alfvén velocity, maximum beam ion velocity, volume averaged fast ion beta, $\langle\beta_{\text{fast}}\rangle$ and total volume averaged beta, $\langle\beta_{\text{total}}\rangle$ from each interval were collected into a database. The parameter $\langle\beta_{\text{fast}}\rangle/V_{\text{Alfvén}}$

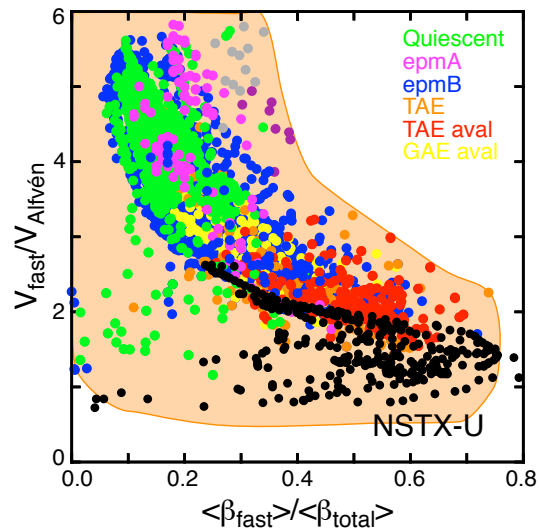


Fig. 1. The colored points are data from NSTX for a variety of fast-ion instabilities, the tan region corresponds to the approximate parameter range expected for NSTX-U. The black points are from initial NSTX U shots.

$\langle\beta_{\text{total}}\rangle$ was found to be useful for predicting the regimes where TAE avalanches and quiescent plasmas were found (Fig. 1). The original NSTX database has been extended to include q-profile from MSE-constrained equilibrium construction and information from the rotation profile measured with the CHERs diagnostic, which could be important for predicting stability of various modes. The original database was based on the list of shots from the 2010 campaign for which TRANSP runs had been done. The database parameters were extended by using the shots which had MSE-constrained equilibrium reconstructions.

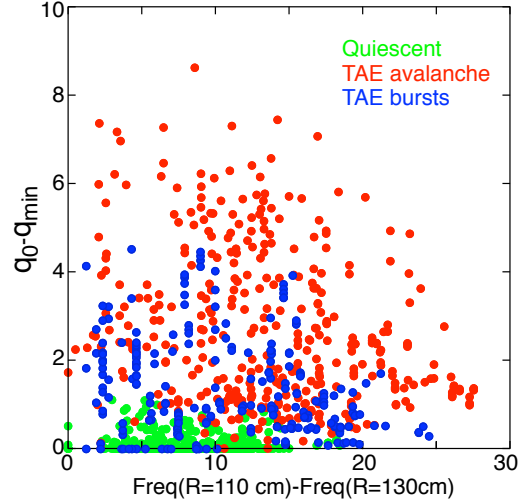


Fig. 2. Existence plot for TAE, TAE avalanches and quiescent plasmas seen on NSTX vs. core shear and rotational shear.

2. Construction of database

Anecdotally, the TAE avalanches that have been chosen for careful study have all had shear-reversal near the axis, that is the minimum in the q-profile was off the magnetic axis. Our present theoretical understanding of TAE stability, and avalanching, is not refined enough to suggest why shear reversal, as opposed to just low shear, seems to enable TAE avalanching. We look for correlations with the magnetic shear on axis in a broader range of shots using the proxy parameter $(q(0) - q_{\min})$, which of course will be zero for normal shear, otherwise it will indicate the extent of shear reversal. Rotational shear can be stabilizing for global modes and we use the parameter $f_{110} - f_{130}$, which is the rotation frequency at $R=1.1\text{m}$ minus the rotation frequency at $R=1.3\text{m}$, radii which typically span the peak in amplitude of TAE (the magnetic axis is typically at $R \approx 1.0\text{m}$). In Fig. 2 we compare those parameters for shots with TAE

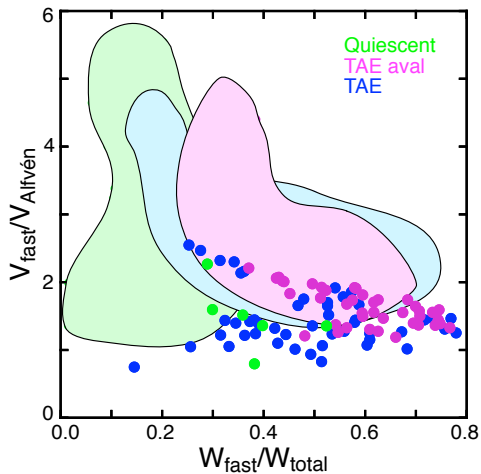


Fig. 3. Existence plot for TAE, TAE avalanches and quiescent plasmas seen on NSTX-U.

bursts (blue), avalanches (red) and shots which are nominally quiescent. The quiescent plasmas tend to have normal magnetic shear, within the reconstruction uncertainties, whereas the avalanching shots tend to have significant core shear reversal. The shots with just ‘bursting’ TAE had a smaller amount of shear reversal, however, the boundary between avalanching and bursting TAE is somewhat arbitrary. The results with rotational shear were contrary to expectations in that the quiescent plasmas had less rotational shear than the plasmas with TAE avalanches, indicating that the levels of rotational shear reached in NSTX were not strongly stabilizing. As these observations

show correlation, not causality, they suggest a directions for future experiments to clarify the relationship.

In Fig. 3 is shown an initial database constructed from NSTX-U of quiescent, TAE and TAE avalanche shots, overlaid on the similar data from NSTX. For the NSTX data set, the parameter $V_{fast}/V_{Alfvén} > 1$ due to the relatively low toroidal field. Nearly all of the NSTX-U shots from the 2016 campaign were taken at a nominal toroidal field of 6 kG, and tended to be at lower density than typical NSTX shots, thus $V_{fast}/V_{Alfvén}$ was extended to significantly lower values

than achieved on NSTX, albeit with limited diagnostic coverage as yet. The NSTX-U data pushes the range of TAE activity to where $V_{fast}/V_{Alfvén} < 1$, but avalanching has not yet been seen for $V_{fast}/V_{Alfvén} < 1$. More importantly, quiescent plasmas were seen at higher values of $\langle \beta_{fast} \rangle / \langle \beta_{total} \rangle$ than on NSTX, suggesting that the curve separating the quiescent regime from the regime with avalanches may also depend of the ratio of $V_{fast}/V_{Alfvén}$.

On NSTX, the variation in fast-ion parameters from the three neutral beam sources was relatively small. All three sources had tangency radii inside the magnetic axis and the beam beta was peaked on axis, with relatively similar pitch-angle distribution. The new neutral beam sources extend the parameter range of fast-ion distribution functions available on NSTX-U, generally generating fast-ion distributions with pitch closer to unity, and for at least the furthest outboard source, allowing for beam betas to peak off-axis. Parameters characterizing the distribution function as a function of sources being injected will need to be added. The extension of the quiescent regime to higher $\langle \beta_{fast} \rangle / \langle \beta_{total} \rangle$ seen in Fig. 3 might be a reflection of some differences in the fast-ion distribution function between NSTX and NSTX-U, rather than a dependence on global plasma parameters.

A clear example of this is the discovery of a counter-propagating TAE, found with injection of the furthest outboard neutral beam source

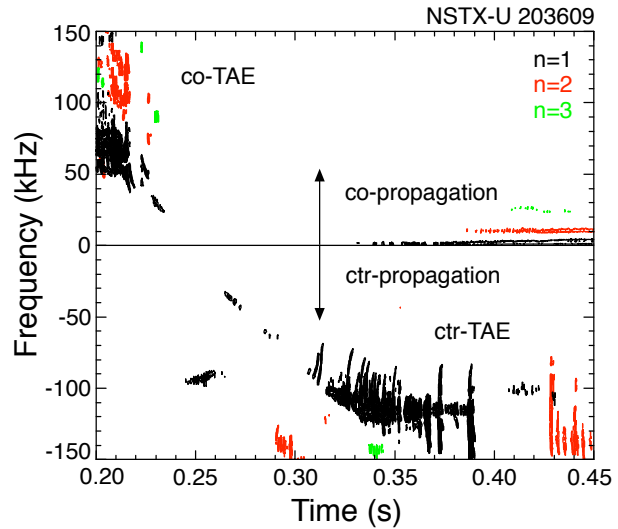


Fig. 4. a) color-coded spectrogram showing TAE activity. Dominant modes are $n=1$ (black), $n=2$, (red). Positive frequencies indicate co-propagation, negative are counter propagation.

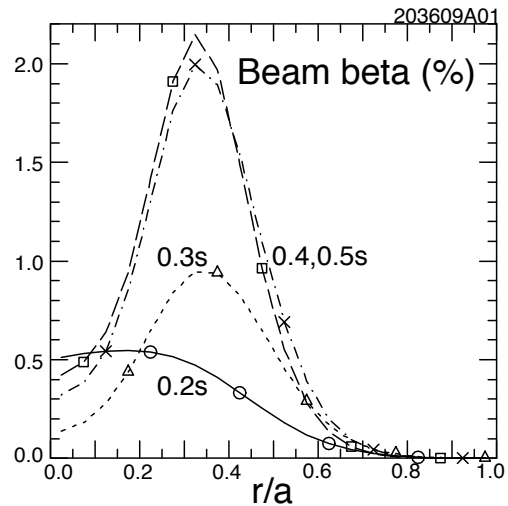


Fig. 5. Profiles of the fast ion beta, as calculated in TRANSP, for the shot in Fig. 4.

(tangency radius of 130 cm) shown in Fig. 4. In the spectrogram shown in Fig. 4, modes that are propagating in the co (with beam) direction are shown with positive frequencies, modes propagating in the counter direction (against the beams) are shown with negative frequency. The colors indicate the toroidal mode numbers as indicated in the figure. The $n=1$ and $n=2$ TAE are initially (*ca.* 0.2s) propagating in the co-direction, as expected for TAE. By 0.31s, the TAE are propagating counter to the beam injection direction.

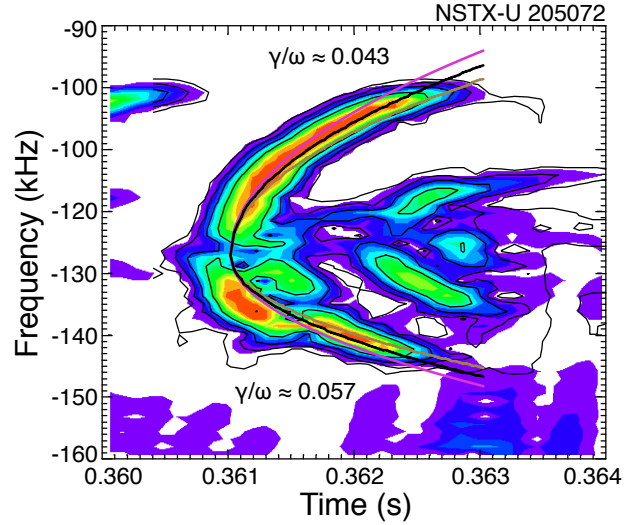


Fig. 6. a) spectrogram showing single burst of a counter-propagating TAE, with both up and down frequency chirping.

Counter-propagating TAE were predicted previously [4] for a hollow fast ion profile. For the example in Fig. 3, the TRANSP prediction of the fast-ion beta profile is shown in Fig. 4. The profile starts out peaked on axis at 0.2s, but is quite hollow by 0.3s, about the time the counter-propagating TAE appear. The off-axis peak in the fast ion beta is located at about the tangency radius for the beam being injected.

The counter-propagating TAE tend to chirp in both directions, and an estimate of the growth rate can be made by fitting the frequency chirp to the formula [4] $\omega = \omega_0 \pm 0.44\gamma_L(\gamma_D t)^{1/2}$ with the assumption that $\gamma_L \approx \gamma_D$ as is shown in Fig. 6 (from a different shot than shown in Figs. 4 & 5). The estimate of the growth rate is comparable to the estimate for normal TAE on NSTX, indicating that the drive for these modes is comparable to that for co-propagating modes. These particular TAE did not avalanche, however, in the 2016 NSTX-U campaign, only three shots were found with this type of TAE and all three shots had only the outermost neutral beam on at the time. Perhaps with more power, the ctr-TAE can also be made to avalanche.

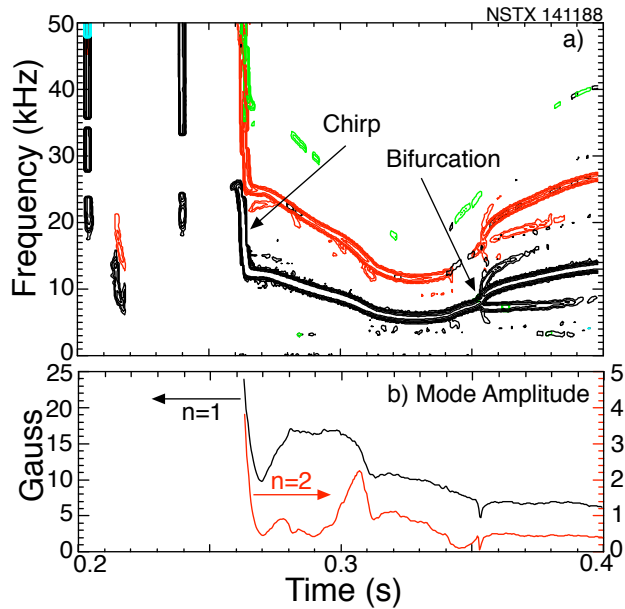


Fig. 7. a) Spectrogram showing onset of epMB with “chirp”, followed by bifurcation at 0.35s, b) amplitude evolution of $n=1$ (black) and $n=2$ (red) modes.

3. Energetic particle modes, kinks and bifurcation

There are a variety of instabilities excited in the range of frequencies well below the TAE frequency in spherical and conventional tokamaks. These include a variety of ‘fishbone’ modes [5], saturated fishbone modes, beta-induced Alfvén eigenmodes, and kinetic ballooning modes. On NSTX and NSTX-U, the frequency separation between modes like fishbones and TAE is not so large. With unbalanced co-NB injection the Doppler correction to the TAE frequency can easily be larger than the TAE frequency itself, pushing fishbone frequencies up towards the TAE frequency

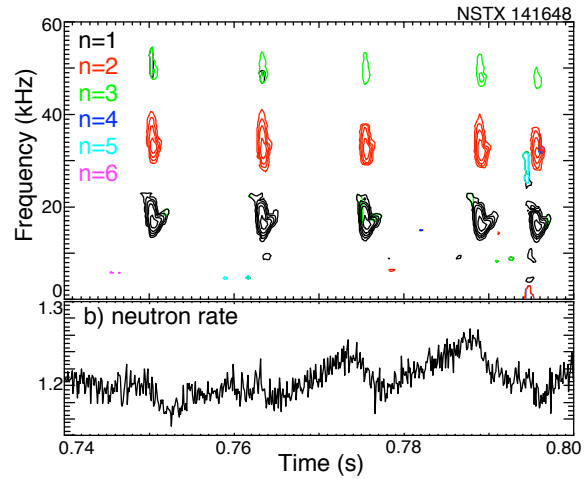


Fig. 8. a) fishbone-like Energetic Particle Modes (epmA), b) neutron rate (a.u.).

gap. Further, the sheared rotation profile often means that the TAE which have frequencies in the TAE-gap at the half radius, can have zero or negative frequency in the plasma frame on the magnetic axis. This makes identification of modes based solely on the frequency spectrum more difficult on NSTX and beam-heated ST's than in conventional tokamaks. In the spectrogram shown in Fig. 7 you can see at ≈ 0.21 s a TAE burst which chirps downwards in frequency until the mode frequency is in the range of MHD kink frequencies.

For the identification of modes in the database, downward chirping modes where the onset frequency was well below the TAE frequency, were identified generically as Energetic Particle Modes, that is, modes with physics similar to that of the fishbone instability. In the

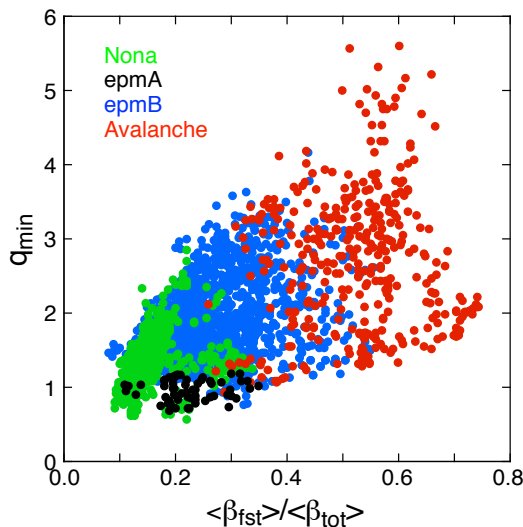


Fig. 9. Database showing existence of TAE avalanches (red), epmB (blue), epmA (black) and quiescent plasmas.

frequency spectra, two qualitatively different behaviors were seen, and labeled as epmA and epmB. The epmA appeared very similar to the classical fishbone first seen on conventional tokamaks and typical examples from NSTX are shown in Fig. 8. The second type, epmB, start with a very similar frequency chirp, but rather than fading away at the bottom of the frequency chirp, the mode persists for up to 100's of ms as is seen for the mode in Fig. 7 at 0.26s. In this section, we will provide more detailed experimental descriptions of the epmA and epmB modes, as well as plasma parameters where they are found.

In Fig. 9 is shown an existence plot for the

epmA (black), epmB (blue) as well as TAE avalanches (red) and quiescent plasmas (green) in the space of q_{min} vs $\langle\beta_{fast}\rangle/\langle\beta_{total}\rangle$. In this dataset the fishbone-like modes (black dots) are found with $q_{min} \approx 1$, and for relatively low $\langle\beta_{fast}\rangle/\langle\beta_{total}\rangle$. Quiescent plasmas (not counting GAE or CAE activity) are found when $\langle\beta_{fast}\rangle/\langle\beta_{total}\rangle < 0.3$ and for $1 \leq q_{min} \leq 3$. So far, no correlation of high rotational shear has been found with quiescent plasmas, however, the rotation profile still useful for mapping the radial location of some modes.

2.1 epmA (fishbone modes)

Fishbone-like modes are relatively common on NSTX, however they tend to appear under qualitatively different circumstances than in conventional tokamaks. On conventional tokamaks, fishbones often appear towards the end of the sawtooth cycle as a relatively repetitive instability. Sawtoothing plasmas on NSTX were extremely rare, even in cases like these where the measured $q(0) \approx 1$ (Fig. 6, black points). Fishbones on NSTX tend to appear more sporadically. They may be isolated, as in Fig. 8, or appear in the presence of TAE, kinks or other MHD activity. They often cause significant drops in the neutron rate (Fig. 8) indicating, as on conventional tokamaks, showing that they cause substantial fast-ion losses.

Early studies of fishbone-like epms on NSTX found that they were likely driven through a bounce-resonance with the fast ions. A similar study was done of potential resonances for one of the cases in this database. The ORBIT code was used to calculate the precession and bounce frequencies for fast ions as a function of their midplane birth radius and pitch. The TRANSP fast ion distribution function at this time are peaked near a pitch of ≈ 0.5 over this range of radii. As can be seen in Fig. 10, the bounce frequencies (red curves) are much higher than the measured epmA frequency, closer to the TAE frequency range. However, as in conventional aspect ratio tokamaks, the precession frequencies cover the range of the epmA frequency chirp. Thus, in this case, the epmA are essentially classical fishbones.

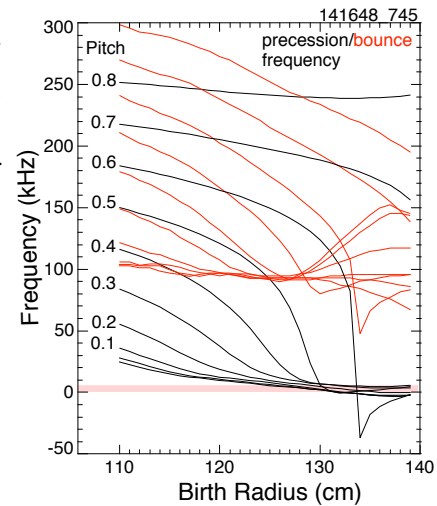


Fig. 10. Calculated precession frequencies (black) for 45kV fast ions using the ORBIT code. Also shown are the bounce frequencies.

2.2 epmB (Long-lived modes)

The modes designated epmB are in many aspects very similar to the Long-Lived-Mode (LLM) reported on MAST [6]. As on MAST, the modes were marked by a fast downward frequency chirp or sweep, very reminiscent of the frequency chirp of the fishbone. The modes are believed to be ideal, largely because they often become stable after 10 to 100msec. The neoclassical drive is calculated to be growing as the mode becomes stable. As in MAST, it is not understood why

the long-lived kink mode doesn't force reconnection leading to a large neoclassical tearing mode.

At the onset of the epMB, the frequency chirps downward (Fig. 11a) and the core rotation profile collapses (Fig. 11b). as was reported on MAST. The range of the frequency chirp at the onset of long-lived modes is larger than the measured frequency change of the on-axis rotation, and the frequency drop off-axis is less, thus some of the frequency chirp may be due to fast particle effects. Occasionally, some 10's of msec later, but not always, the mode bifurcates into a low and high frequency branch. This bifurcation is accompanied by a re-peaking of the core rotation, presumably as the rotation sheared the kink into two separate modes, one localized in the core region, the other farther out.

The onset of the epMB is only weakly correlated with q_{min} passing through a low-order rational surface. In Fig. 12 is shown a histogram of q_{min} 's at the onset of epMB's in this dataset (blue). There is a weak peaking around $q_{min} \approx 2.2$ and 3.3 as might be expected for infernal modes, but the correlation with low-order rational surfaces is not strong. The mode frequency evolution was tracked at 10

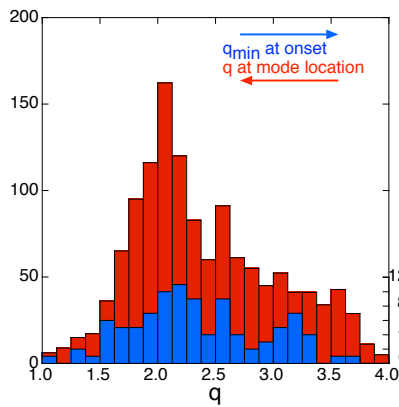


Fig. 12. Histograms of q_{min} at mode onset (blue) and q at the radius where plasma toroidal rotation matched the mode frequency.

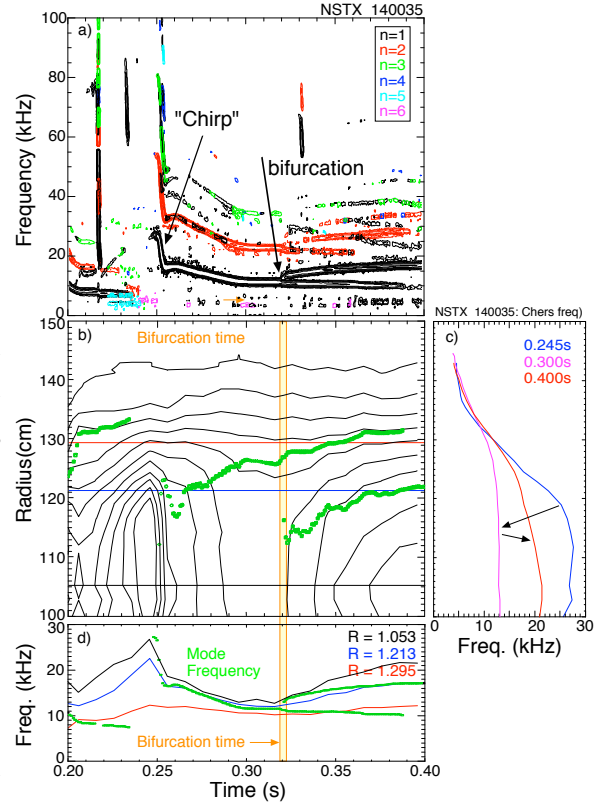


Fig. 11. a) spectrogram showing epmB and harmonics, b) Contours of the toroidal rotation profile showing effect of mode in Fig. 3 on core rotation. Green lines show where mode frequency matches plasma rotation. c) profiles of rotation from before collapse, during core flattened period and after recovery, d) rotation at the three radii indicated.

ms intervals, and the mode frequency was mapped to the plasma rotation, and then to the local q . That data is shown as the red histogram in Fig. 12. Now, the correlation with the $q=2$ rational surface is stronger, but the distribution is still quite broad. The weak peaks near $q=2.5$, $q=3$ and $q=3.5$ are probably not statistically significant. A strong correlation would be expected if a 2/1 island had formed, which would tend to lock the mode to the plasma rotation at the island rational surface.

We use the mode frequency to identify the radial location of the modes (Fig. 13b), and the equilibrium construction, constrained with MSE data, to get q at the mode location

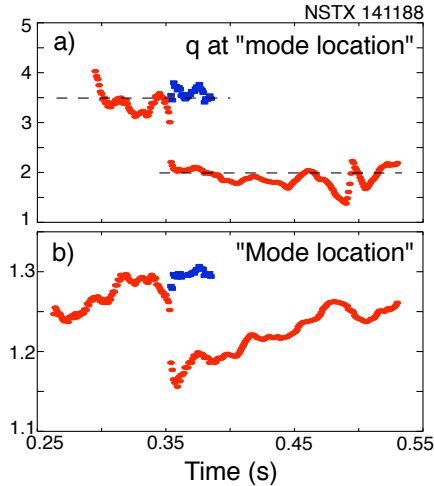


Fig13. a) local value of q at the $n=1$ mode location for the epMB shown in Fig. 7, red is the dominant mode, blue the bifurcated mode, b) radial location of the $n=1$ modes in Fig. 7.

all of the modes is modulated, similar to the case for the ‘pitchfork modes’ [7]. This might support a contention that fast-ions provide some of the drive for these modes. Note that the dominant $n=2$ (red) mode is not at twice the $n=1$ frequency, thus is probably a mostly independent mode.

NSTX-U, which sees a broad spectrum of modes excited by the neutral beam ions, provides an excellent laboratory to improve our understanding of the physics of energetic particle driven instabilities and to develop tools to control these instabilities and predict their effect on ITER and other fusion devices.

Work supported by U.S. DOE Contract DE-AC02-76CH03073.

Appendix:

- [1] M. Ono, S. M. Kaye, Y.-K. M. Peng, *et al.*, Nucl. Fusion **40**, 557 (2000).
- [2] E D Fredrickson, N N Gorelenkov, *et al.*, Nucl. Fusion **54** (2014) 093007.
- [3] H.V. Wong, H. L. Berk, Phys. Lett. A **251** (1999) 126.
- [4] H L Berk, B N Breizman, and N V Petviashvili, Phys. Lett. A **234** (1997) p213.
- [5] F. Zonca, L. Chen, A. Botrugno, *et al.*, Nucl. Fusion **49**, 085009 (2009).
- [6] I T Chapman, M-D Hua, S D Pinches, *et al.* Nucl. Fusion **50** (2010) 045007
- [7] A. Fasoli, D. Borba, C. Gormazano, *et al.*, PP&CF **39** (1997) B287.

(Fig. 13a). Here red indicates the dominant mode, blue, the lower frequency, bifurcated mode. After the bifurcation, at the inferred dominant mode location $q \approx 2$, and at the weaker mode location $q \approx 3.5$, although within the uncertainty this could be $n=3$ or $n=4$.

Something resembling the opposite of this bifurcation has also been seen, but the cause may be different. In Fig. 14 is shown a spectrogram showing the onset of a similar low-frequency mode. The spectrum could be interpreted as multiple $n=1$ modes at different frequencies, coalescing to one mode at about 0.69s, however it seems unlikely that that many different modes would simultaneously become unstable. The

amplitude envelope of

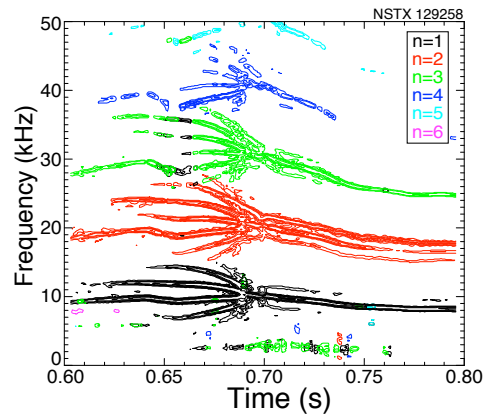


Fig. 14. Spectrogram showing onset of kink-like mode showing what appears to be a coalescence of multiple modes. It is unclear whether the higher n modes are independent of the $n=1$ kink mode.